# Anharmonic interatomic potentials of octahedral Pt-halogen complexes studied by extended x-ray-absorption fine structure

Toshihiko Yokoyama, Yoshiki Yonamoto, and Toshiaki Ohta
*Department of Chemistry, Graduate School of Science, The University of Tokyo, 7-3-1 Hongo, Bunkyo-ku, Tokyo 113, Japan*

Akito Ugawa
*Institute for Molecular Science, Myodaiji, Okazaki, Aichi 444, Japan*
(Received 7 March 1996)

The temperature dependence of Pt $L_{\mathrm{III}}$- and I $K$-edge extended x-ray-absorption fine-structure spectra of octahedrally coordinated Pt $X_6^{2-}$ ($X=$ Cl, Br, and I) complexes has experimentally been investigated not only for the first-nearest-neighbor (NN) shells but for higher NN ones. The second- and third-order cumulants of a radial distribution function in the octahedral system have been evaluated quantum mechanically by employing the interatomic potential including the third-order force constants. The experimentally obtained second-order cumulants agree with the values expected by the vibrational data and the third-order cumulants have successfully given the anharmonic force constants. Contribution of the bending motions to the cumulants of higher NN shells is discussed in detail. [S0163-1829(96)04934-X]

## I. INTRODUCTION

Extended x-ray-absorption fine-structure (EXAFS) spectroscopy has widely been utilized for structure analysis in various fields of science.[1] EXAFS contains information on local structures around x-ray-absorbing atoms, and usually gives coordination numbers and interatomic distances. Recently thermal motions have also become an attractive subject, which are given in higher-order moments of radial distribution functions. In order to treat asymmetric radial distribution functions due to anharmonicity, the cumulant-expansion technique[2] has been exploited as the most practical method and has extensively been used in moderately disordered systems for bulk[3] and surface materials.[4] The next step for further understanding of the disorder problem is to know direct relationship between the interatomic potential and the cumulants. Recently Rabus[5] and Frenkel *et al.*[6] have derived quantum-mechanical formulas including third-order anharmonicity for a simple diatomic system, while Miyanaga and Fujikawa[7] have extended the theory to a one-dimensional infinite chain including the third- and fourth-order cumulants.

In our previous study,[8] we have derived the formulas of the cumulants for a linear triatomic system and analyzed the temperature-dependent EXAFS spectra of diatomic $Br_2$, and linear triatomic $HgBr_2$, $HgCl_2$, $AuBr_2^-$, and $CuBr_2^-$. The anharmonic interatomic potentials have subsequently been determined from the obtained cumulants, and it has been emphasized that the many-atom treatment is essentially important to describe the thermal motions especially for the higher nearest-neighbor (NN) shells which have no chemical bonds with the x-ray-absorbing atom. In the linear molecular systems, the bending vibrational motion does not contribute to the cumulants within the first-order approximation, because the displacement vector for the bending motion is perpendicular to any bond direction. Since one should take account of only the stretching motions in the linear molecules, this yields significant simplification for the description of temperature dependence of EXAFS spectra. On the contrary, for all the other point-group systems, generally speaking, the bending motions should be taken into account beyond the first-NN shell. It has not yet been investigated whether the bending anharmonicity is important to describe the cumulants, although this should be an essential problem for further understanding of EXAFS spectroscopy.

In the present study, we have carried out quantum statistical calculations to derive the cumulants of the octahedrally coordinated system including the third-order anharmonicity in the interatomic potential. We have measured and analyzed the temperature dependence of Pt $L_{\mathrm{III}}$- and I $K$-edge EXAFS spectra of a $PtI_6^{2-}$ complex not only for the first-NN shell but for the second- and third-NN ones. We have also investigated Pt $L_{\mathrm{III}}$-edge EXAFS of other octahedral Pt halogen complexes of $PtCl_6^{2-}$ and $PtBr_6^{2-}$ for comparative discussion. We will finally conclude whether only the stretching motion is necessary or the bending motion is also important to yield proper cumulants.

In Sec. II of this work, we briefly describe the experimental details on EXAFS and far-infrared spectroscopic measurements. Section III deals with the vibrational analysis to give the second-order force constants within the harmonic approximation, and the evaluation of the cumulants using the third-order anharmonic potential by applying the first-order perturbation theory of thermal averages. Section IV gives the results and discussion of the EXAFS analysis for the static structure analysis as well as the temperature dependence. Section V summarizes the concluding remarks.

## II. EXPERIMENT

Temperature dependence of Pt $L_{\mathrm{III}}$-edge EXAFS spectra of $K_2PtCl_6$, $K_2PtBr_6$, and $K_2PtI_6$ was investigated at BL-10B (Ref. 9) of the Photon Factory in the National Laboratory for High Energy Physics (KEK-PF, the ring energy of 2.5 GeV and the stored ring current of 350–250 mA), while I $K$-edge EXAFS of $K_2PtI_6$ was taken at BL-7C (Ref. 10) of KEK-PF

 

with the operating ring energy of 3.0 GeV and the stored current of 170–150 mA. All the EXAFS spectra were recorded with the transmission mode using a Si(311) channel-cut (BL10B) or double-crystal (BL7C) monochromator. Ionization chambers were employed for the measurements of intensities of incident ($I_0$) and transmitted ($I$) x rays, which were filled with $N_2$ and Ar, respectively, for the Pt $L_{III}$-edge EXAFS. In the case of I $K$-edge EXAFS, we used Ar and Kr gases for $I_0$ and $I$ ionization chambers, respectively. Data acquisition periods were 1 s/point for Pt $L_{III}$ edge and 2 s/point for I $K$-edge EXAFS.

Commercially available $K_2PtCl_6$, $K_2PtBr_6$, and $K_2PtI_6$ were used without further purification. The samples were diluted with boron nitride, pressed to make disks with a diameter of 12 mm, and cooled down to the temperatures using a closed-cycle refrigerator. Measurement temperatures $T$ are listed in Figs. 2, 4, and 5 described below. The absorption jumps at the edges were less than 1.5 for all the samples, implying fewer effects of higher harmonics in the present ring energy of 2.5 GeV for Pt $L_{III}$ edge or 3.0 GeV for I $K$ edge. The sample temperature was monitored by an electric resistance of a Si diode placed closely to the sample disk.

Because of a lack of vibrational spectra of the $PtI_6^{2-}$ system, we have carried out the measurements of a far infrared spectrum of $K_2PtI_6$. The spectrum was recorded in a similar manner described previously.[8]

## III. THEORY

### A. Dynamical matrix calculation

Prior to the calculation of the cumulants, one has to determine the nonperturbed eigenvalues and eigenfunctions within the framework of harmonic oscillators. Here we assume an octahedral system $MX_6$ with atomic masses $M$ and $m$ for central atom $M$ and terminal atom $X$, respectively. To solve the dynamical matrix, we use the simple Urey-Bradley force field,[11] whose **G** and **F** matrices for each symmetry can be given as[12]

$$
\begin{aligned}
&A_{1g}: \quad \mathbf{G}(A_{1g})=\mu_B, \quad \mathbf{F}(A_{1g})=K+4F,\\
&E_g: \quad \mathbf{G}(E_g)=\mu_B, \quad \mathbf{F}(E_g)=K+0.7F,\\
&F_{1u}: \quad \mathbf{G}(F_{1u})=\begin{pmatrix} 2\mu_A+\mu_B & -4\mu_A\tau \\ -4\mu_A\tau & 2(4\mu_A+\mu_B)\tau^2 \end{pmatrix}, \quad \mathbf{F}(F_{1u})=\begin{pmatrix} K+1.8F & 0.9r_0F \\ 0.9r_0F & r_0^2(H+0.55F) \end{pmatrix},\\
&F_{2g}: \quad \mathbf{G}(F_{2g})=4\mu_B\tau^2, \quad \mathbf{F}(F_{2g})=r_0^2(H+0.55F),\\
&F_{2u}: \quad \mathbf{G}(F_{2u})=2\mu_B\tau^2, \quad \mathbf{F}(F_{2u})+r_0^2(H+0.55F),
\end{aligned}
\tag{1}
$$

where $\mu_A=1/M$, $\mu_B=1/m$, $\tau=1/r_0$, and $r_0$ is the equilibrium $M$-$X$ distance. $K$, $F$, and $H$ are the second-order force constants for $M$-$X$ stretching, $X$-$X'$ interaction, and $X$-$M$-$X'$ bending modes. The basis set for the above **GF** matrices is the internal symmetric coordinate **S**, which is given by a unitary transformation of the original internal vectors **X** of the $M$-$X$ distance displacements ($\Delta r_l$) and the $X$-$M$-$X'$ angle displacements ($r_0\Delta\phi_{lm}$), the dimension of the internal coordinate **X** or **S** being 18 including 3 rotational freedoms.

Since vibrational spectra directly give the eigenvalues of the **GF** matrix, one can obtain the force constants $K$, $F$ and $H$, and the normal coordinate **Q** which is given by the linear combination of **X** as

$$\mathbf{X}=\mathbf{eQ}, \tag{2}$$

where **e** is the transformation matrix. Raman and infrared spectroscopic data of $PtCl_6^{2-}$ and $PtBr_6^{2-}$ can be referred to in the literature,[13] while the infrared spectrum of $PtI_6^{2-}$ was measured in this study. The resonance frequencies for $PtI_6^{2-}$ were found at 185.5 and 84.9 $cm^{-1}$. The former is assigned to the antisymmetric stretching mode ($f_{1u}$) and the latter to the bending mode ($f_{1u}$). Because the Raman data of $PtI_6^{2-}$ are not available, we use the present EXAFS results of $\Delta C_2$ for the first-NN Pt-I shell described below, in order to calculate the force constants $K$, $F$, and $H$. The results of the force constants are summarized in Table II discussed below, and the obtained normal coordinate **Q** will be used to calculate the cumulants.

### B. Cumulant evaluation

Let us evaluate the first- to third-order cumulants for the system including the third-order anharmonic potential. We will describe the interatomic potential $V$ in terms of **Q** such that

$$V=\tfrac{1}{2}\sum_p \omega_p^2Q_p^2-\sum_{p\leqslant q\leqslant r}\alpha_{pqr}Q_pQ_qQ_r, \tag{3}$$

where the first term corresponds to the harmonic potential ($\omega_p$ is the $p$th normal vibrational frequency) and the second term can be regarded as a perturbed Hamiltonian $H'$, in which $\alpha_{pqr}$ is the third-order force constant.

In order to evaluate the second-order cumulants $C_2$, one can use the harmonic approximation because the odd-order terms do not contribute to the even-order moments within the first-order perturbation theory. The thermal average of $Q_iQ_j$ is known to be simply given as

$$\langle Q_iQ_j\rangle=\frac{\hbar}{2\omega_i}\frac{1+z_i}{1-z_i}\delta_{ij}=\sigma_i^2\frac{1+z_i}{1-z_i}\delta_{ij}, \tag{4}$$

where $\hbar$ is the Planck constant divided by $2\pi$, $\delta_{ij}$ the Kronecker's delta function, $\sigma_i^2$ is the zero-point vibrational amplitude of the $i$the mode, and $z_i = \exp[-\hbar\omega_i/k_BT]$ ($k_B$ the Boltzmann constant and $T$ the temperature).

The first- and third-order cumulants $C_1$ and $C_3$ can be calculated using the first-order perturbation formula of thermal averages.[6,8] The third-power moment $\langle Q_iQ_jQ_k\rangle$ is given as

$$\langle Q_iQ_jQ_k\rangle = \frac{1}{Z_0}\sum_{p\le q\le r}\sum_{n,n'}\frac{z^n - z^{n'}}{E_n - E_{n'}} \times\langle n|Q_iQ_jQ_k|n'\rangle\langle n'|-\alpha_{pqr}Q_pQ_qQ_r|n\rangle = \sum_{p\le q\le r} Q^{(3)}_{ijk,pqr}\alpha_{pqr}, \tag{5}$$

where $Z_0$ is the partition function of the nonperturbed system, and $E_n$ the eigenvalue of the nonperturbed state $n$. The state $n$ contains 15 vibrational quantum numbers $n=(n_1,n_2,\ldots,n_{15})$ in the octahedral system, some of the levels being energetically degenerated. Although the analytical calculation of $Q^{(3)}$ is a tedious task, one can classify three different cases as follows. For $i\neq j\neq k$, when $p=i$, $q=j$, and $r=k$, one obtains a nonzero value as

$$Q^{(3)}_{ijk,pqr} = \frac{2\sigma_i^2\sigma_j^2\sigma_k^2}{(1-z_i)(1-z_j)(1\text{-}z_k)}\left\{\frac{1-z_iz_jz_k}{\hbar(\omega_i+\omega_j+\omega_k)} + \frac{z_k-z_iz_j}{\hbar(\omega_i+\omega_j-\omega_k)} + \frac{z_j-z_iz_k}{\hbar(\omega_i-\omega_j+\omega_k)} + \frac{z_i-z_jz_k}{\hbar(-\omega_i+\omega_j+\omega_k)}\right\}, \tag{6}$$

Because $i,j$ and $k$ are mutable with each other, the same expression is valid for $Q^{(3)}_{jik,pqr}$, etc. For $i\neq j=k$, three cases give nonzero values as in Eqs. (7)–(9): when $p=i, q=r=j$ or $r=i, p=q=j$,

$$Q^{(3)}_{ijj,pqr} = \frac{2\sigma_i^2\sigma_j^4}{(1-z_i)(1-z_j)^2}\left\{\frac{(1-z_i)(1+6z_i+z_i^2)}{\hbar\omega_i} + \frac{2(1-z_iz_j^2)}{\hbar(\omega_i+2\omega_j)} + \frac{2(z_i-z_j^2)}{\hbar(-\omega_i+2\omega_j)}\right\}, \tag{7}$$

when $p=q=r=i$,

$$Q^{(3)}_{ijj,pqr} = \frac{6\sigma_i^2\sigma_j^4}{\hbar\omega_i}\frac{1+z_i}{1-z_i}\frac{1+z_j}{1-z_j}, \tag{8}$$

and when $p=i$, $q=r\neq i$, $\neq j$, or $r=i$, $p=q\neq i$, $\neq j$

$$Q^{(3)}_{ijj,pqr} = \frac{2\sigma_i^2\sigma_j^2\sigma_q^2}{\hbar\omega_i}\frac{1+z_j}{1-z_j}\frac{1+z_q}{1-z_q}. \tag{9}$$

For $i=j=k$, two cases show nonzero values: when $p=q=r=i$

$$Q^{(3)}_{iii,pqr} = \frac{2\sigma_i^6}{\hbar\omega_i}\frac{11+38z_i+11z_i^2}{(1-z_i)^2}, \tag{10}$$

and when $p=i$, $q=r\neq i$, $\neq j$ or $r=i$, $p=q\neq i$, $\neq j$,

$$Q^{(3)}_{iii,pqr} = \frac{6\sigma_i^4\sigma_q^2}{\hbar\omega_i}\frac{1+z_i}{1-z_i}\frac{1+z_q}{1-z_q}. \tag{11}$$

All the other elements vanish in Eq. (5). For the first-order cumulant $C_1$, which is defined as the thermal average of the distance displacement with respect to the equilibrium distance (the potential minimum), $\langle Q_i\rangle$ is similary given as

$$\langle Q_i\rangle = \sum_{p\le q\le r} Q^{(1)}_{i,pqr}\alpha_{pqr}, \tag{12}$$

where $Q^{(1)}_{i,pqr}$ gives nonzero values when $p=q=r=i$

$$Q^{(1)}_{i,pqr} = \frac{6\sigma_i^4}{\hbar\omega_i}\frac{1+z_i}{1-z_i}, \tag{13}$$

and when $p=i$, $q=r\neq i$, or $r=i$, $p=q\neq i$,

$$Q^{(1)}_{i,pqr} = \frac{2\sigma_i^2\sigma_q^2}{\hbar\omega_i}\frac{1+z_q}{1-z_q}. \tag{14}$$

All the other elements vanish in Eq. (12).

Using these elements [Eqs. (6)–(11), (13) and (14)], one can numerically evaluate $C_1$ and $C_3$ for any NN shell. For this purpose, one should define the third-order force constants in Eq. (3). In the case of the octahedral system, let us assume the anharmonic perturbed Hamiltonian as

$$H' = -\sum_l K_3\Delta r_l^3 - \sum_{lmn} F_{3,lmn}\Delta r_l\Delta r_m\Delta r_n - \sum_{lm} H_3(r_0\Delta\phi_{lm})^3, \tag{15}$$

where $K_3$, $F_3$, and $H_3$ are the third-order force constants. The first and third terms correspond to the anharmonicity due to the stretching and bending motions, respectively. The second one is the cross term between the stretching motions, while the cross terms containing the bending motions are all neglected. Although several types of $F_3$ might exist depending on $l$, $m$, and $n$, we will afterward give some assumptions to fit the experimental data. Using $\mathbf{X}=\mathbf{eQ}$, the force constant $\alpha_{pqr}$ in Eq. (3) can be obtained.

Finally one can evaluate the cumulants. For instance, the first- to third-order cumulants for the second-NN $X$-$X$ shell are given as

$$C_1 = \tfrac{1}{12}\sum_{lm}\langle\Delta r_{lm}\rangle,$$

$$C_2 = \tfrac{1}{12}\sum_{lm}\langle(\Delta r_{lm}-C_1)^2\rangle \cong \tfrac{1}{12}\sum_{lm}\langle\Delta r_{lm}^2\rangle, \tag{16}$$

$$C_3 = \tfrac{1}{12}\sum_{lm}\langle(\Delta r_{lm}-C_1)^3\rangle \cong \tfrac{1}{12}\sum_{lm}\langle\Delta r_{lm}^3\rangle - 3C_1C_2,$$

where

$$\Delta\eta_m = \frac{\Delta r_l+\Delta r_m+r_0\Delta\phi_{lm}}{\sqrt{2}}. \tag{17}$$

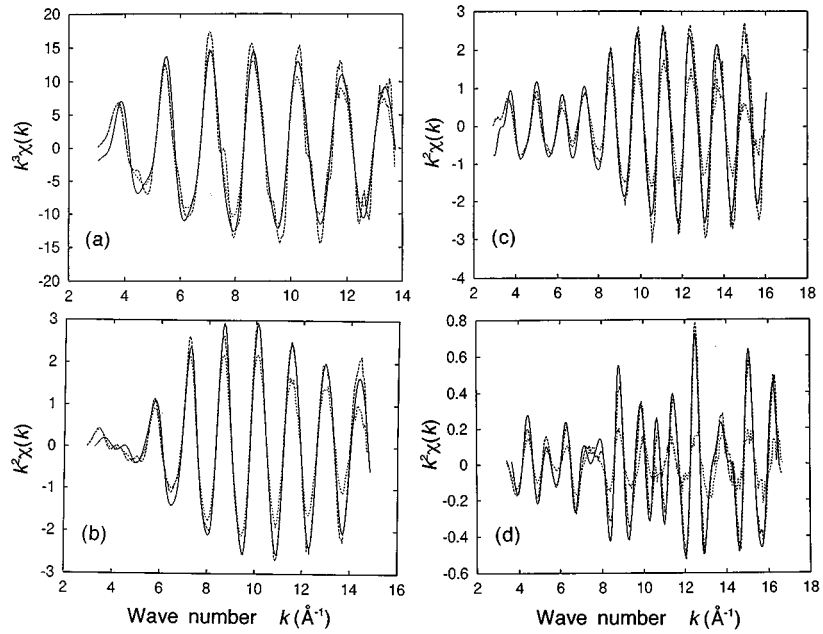


FIG. 1. (a) $L_{\mathrm{III}}$-edge EXAFS oscillation function $k^2\chi(k)$ of $K_2PtCl_6$ at 25 K (long-dashed line) and 300 K (short-dashed), together with the FEFF6 calculation at 25 K (solid); (b) Pt $L_{\mathrm{III}}$-edge $k^2\chi(k)$ of $K_2PtBr_6$ at 71 K (long-dashed) and 300 K (short-dashed) with the calculation at 71 K (solid); (c) Pt $L_{\mathrm{III}}$-edge $k^2\chi(k)$of $K_2PtI_6$ at 38 K (long-dashed) and 300 K (short-dashed) with the calculation at 38 K (solid); (d) I $K$-edge $k^2\chi(k)$ of $K_2PtI_6$ at 50 K (long-dashed) and 300 K (short-dashed) with the calculation at 50 K (solid).

Since $\Delta r_l$, $\Delta r_m$, and $\Delta\phi_{lm}$ are expressed by **e** and **Q**, numerical values of $C_1$, $C_2$,and $C_3$ are obtained straightforwardly using Eqs. (4)–(15). Note that although the octahedral system is assumed here, these expressions in Eqs. (3)–(14) are completely general for any molecular structure and one should rewrite only final expressions as Eqs. (15)–(17). These formulas are employed for the following analysis of the temperature dependence of the experimental EXAFS spectra.

## IV. RESULTS OF EXAFS AND DISCUSSION

### A. Structure analysis

The EXAFS oscillation function $k^n\chi(k)$ was obtained with well-established procedures: pre- and postedge background subtractions and subsequent normalization with the absorption coefficients given in the literature.[1,14] The Pt $L_{\mathrm{III}}$-edge EXAFS functions, $k^3\chi(k)$ of $K_2PtCl_6$ and $k^2\chi(k)$ of $K_2PtBr_6$ and $K_2PtI_6$, and the I $K$-edge function $k^2\chi(k)$ of $K_2PtI_6$ are shown in Fig. 1, including the temperature dependence and the theoretical calculations described below. In all the spectra, the amplitude reduction at higher temperatures can clearly be seen especially at high $k$ regions due to the enhancement of thermal vibration at higher temperatures.

The EXAFS functions were subsequently Fourier transformed into $r$ space (each $\Delta k_{\mathrm{FT}}$ employed is given in Table I, these being depicted in Fig. 2. In all the Pt $L_{\mathrm{III}}$-edge EXAFS two features are found; dominant peaks appearing at ~1.9–2.5 Å can be assigned to the first-NN Pt-$X$ ($X$=Cl, Br, or I) single-scattering path (coordination number $N$=6) and weak features appearing at ~4–5 Å to the multiple-scattering paths. As we have already discussed in the linear triatomic systems,[8] no single-scattering paths within the $PtX_6$ unit can be expected around 4–5 Å, and the weak feature should thus correspond only to the multiple-scattering paths, in which several kinds of Pt-$X$-Pt-$X'$-Pt paths are possible. Dominant contribution is found in the collinear $X$-Pt-$X'$ cases since these paths contain

TABLE I. Results of structural analysis of the EXAFS data of $PtCl_6^{2-}$, $PtBr_6^{2-}$, and $PtI/_6^{2-}$ using theoretical standards given by FEFF6. $R$ denotes the distance given by the crystallographic data, while $R_{\mathrm{ex}}$ is the distance determined by the present EXAFS data. The crystallographic data of $PtBr_6^{2-}$ are not available in the literature. $C_2$ was calculated from the vibrational data. Error bars includes both the experimental and fitting errors, but do not include accuracy of the theoretical standards.

| Sample | Edge | $T$ K | Pair | $\Delta k_{\mathrm{FT}}$ | $\Delta R_{\mathrm{fit}}$ | $\Delta k_{\mathrm{fit}}$ | $S_0^2$ | $R$ (Å) | $R_{\mathrm{EX}}$(Å) | $C_2$ (Å$^2$) |
|---|---|---|---|---|---|---|---|---|---|---|
| $PtCl_6^{2-}$ | Pt-$L_{\mathrm{III}}$ | 25 | Pt-Cl | 3.0–13.7 | 1.65–2.35 | 4.0–13.5 | 0.93(5) | 2.316[a] | 2.318(5) | 0.001 65 |
| $PtBr_6^{2-}$ | Pt-$L_{\mathrm{III}}$ | 71 | Pt-Br | 2.9–14.7 | 1.80–2.60 | 4.0–14.5 | 0.90(5) | | 2.472(5) | 0.001 36 |
| | | | Pt-Br-Pt | 2.9–14.7 | 4.10–5.10 | 5.0–13.0 | 1.04(10) | | 4.932(5) | 0.002 31 |
| $PtI_6^{2-}$ | Pt-$L_{\mathrm{III}}$ | 38 | Pt-I | 2.9–16.0 | 1.95–2.80 | 4.0–16.0 | 0.93(5) | 2.673[b] | 2.673(5) | 0.001 34 |
| | | | Pt-I-Pt | 2.9–16.0 | 4.70–5.40 | 4.0–16.0 | 1.08(10) | 5.346[b] | 5.351(5) | 0.002 04 |
| $PtI_6^{2-}$ | I-K | 50 | I-Pt | 3.4–16.7 | 1.90–2,85 | 4.0–16.0 | 1.12(10) | 2.673[b] | 2.667(5) | 0.001 36 |
| | | | I-I | 3.4–16.7 | 3.10–3.80 | 4.0–16.0 | 1.01(10) | 3.780[b] | 3.773(5) | 0.003 69 |
| | | | I-Pt-I | 3.4–16.7 | 4.60–5.40 | 4.0–16.0 | 1.21(10) | 5.346[b] | 5.338(5) | 0.002 11 |

[a]Reference 16.
[b]Reference 17.

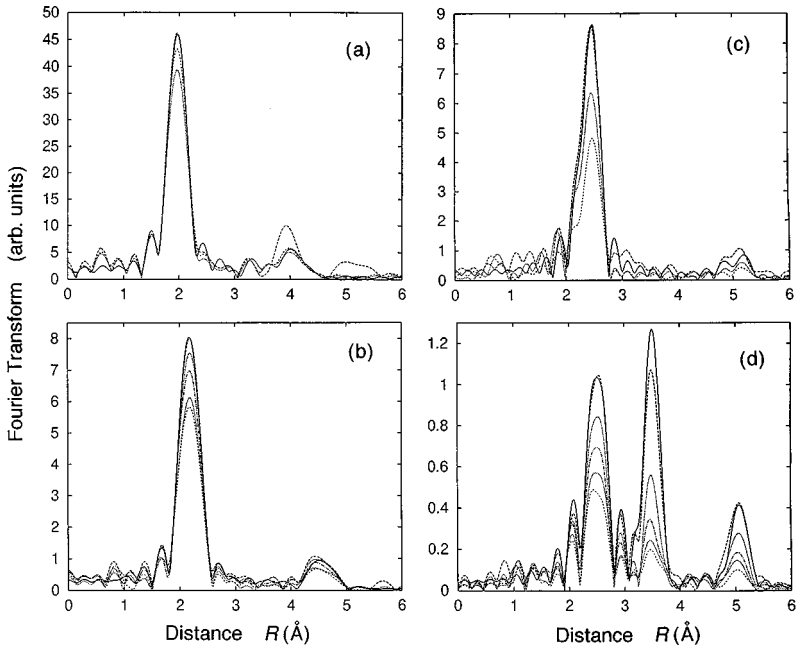


FIG. 2. Fourier transforms corresponding to Fig. 1. (a) $K_2PtCl_6$ (Pt-$L_{III}$) at 25 K (long-dashed), 201 K (short-dashed) and 300 K (dotted), together with the FEFF6 calculation (solid); (b) $K_2PtBr_6$ (Pt-$L_{III}$) at 71 K (long-dashed), 147 K (dotted), 201 K (dot-dashed), 257 K (dotted), and 305 K (short-dashed) with the FEFF6 calculation (solid); (c) $K_2PtI_6$ (Pt-$L_{III}$) at 38 K (long-dashed), 205 K (dotted), and 300 K (short-dashed) with the FEFF6 calculation (solid); (d) $K_2PtI_6$ (I-K) at 50 K (long-dashed), 130 K (dotted), 190 K (dot-dashed), 250 K (dotted), and 300 K (short-dashed) with the FEFF6 calculation (solid).

the focusing forward-scattering effect with Pt, while the other less important paths include the Pt scattering angles of 90° or 180°. Although the Fourier transform concerning I $K$-edge EXAFS of $PtI_6^{2-}$ [Fig. 2(d)] shows more complicated features, the assignments can be done rather straightforwardly; the first peak at ~2.5 Å corresponds to the first-NN I-Pt shell ($N=1$), the second peak at ~3.5 Å to the second NN I-I shell ($N=4$), and the third peak at ~5.1 Å to the I-Pt-I shell. Here we can neglect the double-scattering contribution corresponding to the triangular I-Pt-I′-I path where the I-Pt and Pt-I′ directions are perpendicular to each other. Similarly to the Pt $L_{III}$-edge EXAFS, the observed third peak should contain mainly the collinear cases as the I-I′-I single-scattering (atoms I, Pt, and I′ locate collinearly), the I-Pt-I′-I double scattering (once forward scattering with Pt) and the I-Pt-I′-Pt-I triple scattering (twice forward scattering with Pt). Most features in Figs. 2(c) and 2(d) are accompanied by the side lobes due to nonlinear $k$ dependence of the phase shifts typical for heavy scatterers at Pt and I.

In order to obtain structural parameters and also to verify the reliability of the present theoretical standards, calculations were performed using the FEFF6 program package.[15] This calculation requires only two undetermined parameters to reproduce EXAFS spectra, which are $S_0^2$ and $\Delta E_0$. $\Delta E_0$ is the shift of the edge energy which has tentatively been chosen at the inflection point of the experimental data, and $S_0^2$ is the intrinsic reduction factor of the EXAFS function. The interatomic distances $R$ were taken from the crystallographic data[16,17] and the mean-square relative displacements $C_2$ were calculated from the harmonic vibrational analysis described below. $C_3$ was neglected for simplicity. Since crystallographic data of $PtBr_6^{2-}$ were not available, we used $R$ also as a fitting parameter. Figures 1 and 2 include the results of the FEFF6 calculations for the lowest temperature of the corresponding experimental spectrum. Agreements between the experimental and theoretical spectra are found to be excellent.

A refinement of the interatomic distance was subsequently carried out by means of the single-shell curve-fitting analysis in $k$ space. After the inverse Fourier transformation of the shell of interest, the extracted $k^n\chi(k)$ was fitted using the backscattering amplitude and the phase shift derived by the present FEFF6 calculation. The $\Delta R_{\rm fit}$ and $\Delta k_{\rm fit}$ ranges employed are tabulated in Table I. Here only three fitting parameters of $S_0^2$, $R$, and $\Delta E_0$ were employed ($C_2$ was fixed to the values given by the vibrational analysis), while the number of independent data points estimated by the well-known formula of $N_I=2\Delta k\Delta R/\pi+1$ should be sufficiently larger for all the shells analyzed. Note that here we have allowed $S_0^2$ variation depending on each shell, which was inhibited in the FEFF simulation depicted in Figs. 1 and 2. Conclusively we found excellent agreement with the crystallographic distances not only for the first but for higher NN shells, as shown in Table I, indicating high reliability of the FEFF calculation.

One should, however, be careful to a possible superposition of the $p\rightarrow s$ transition in the Pt $L_{III}$-edge EXAFS analysis since FEFF6 includes only the major $p\rightarrow d$ component. In order to estimate the effect of the $p\rightarrow s$ transition, we have evaluated both the $p\rightarrow s$ and $p\rightarrow d$ component by changing the absorber phase shifts given in the FEFF6 code. It was found that although the phases are noticeably different between each other, the amplitude of the $p\rightarrow s$ component is too small to analyze since the ratio of the transition intensity ($I_{p\rightarrow s}/I_{p\rightarrow d}$) has been assumed to a common value of 0.02.[1] From the curve-fitting analysis including the two components we have found no meaningful differences in the results (the first-NN distance and coordination number differ only by 0.001 Å and 1%, respectively). We can conclusively remark that the above analysis taking account of only the $p\rightarrow d$ component is sufficient for the present discussion. It is also noted that in the present study we have measured both the Pt $L_{III}$- and I $K$-edge EXAFS for $PtI_6^{2-}$ and have obtained the identical results (see Table I and also Fig. 5 and Table II

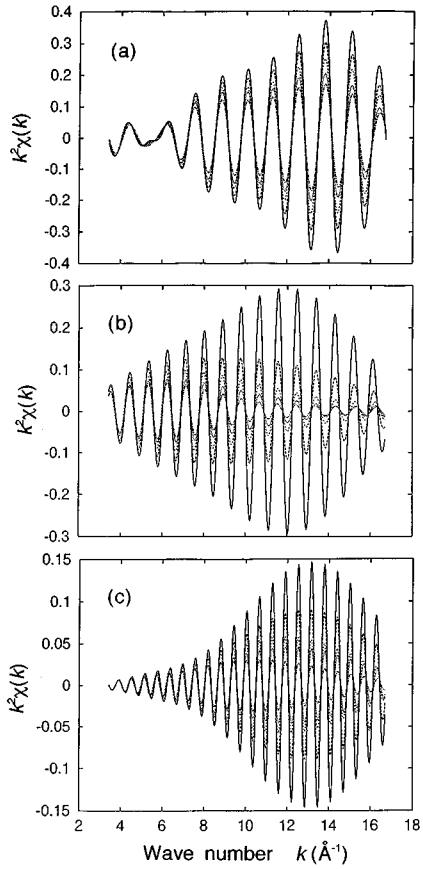


FIG. 3. Filtered $k^2\chi(k)$ of I $K$-edge EXAFS for (a) the first-NN I-Pt shell, (b) the second-NN I-I shell, and (c) the third-NN I-Pt-I shell, at temperatures of 50 K (solid), 130 K (long-dashed), 190 K (short-dashed), 250 K (dotted), and 300 K (dot-dashed).

given below), this justifying the omission of the $p \rightarrow s$ component in the polarization-averaged $L_{\mathrm{III}}$-edge EXAFS.

### B. Analysis of temperature dependence

The temperature dependence of the EXAFS spectra was subsequently analyzed by means of the amplitude-ratio and phase-difference methods or the curve-fitting method. In this analysis, we employed the lowest-temperature data as empirical standards, and therefore we can estimate the difference of the second- and third-order cumulants between the lowest and higher temperatures. The $\Delta R_{\mathrm{fit}}$ and $\Delta k_{\mathrm{fit}}$ ranges were basically the same as in the above structure analysis, and the fitting parameters are $\Delta R$, $\Delta C_2$, and $\Delta C_3$. Since the temperature-dependent analysis requires higher quality of the data than the distance estimation, we have consequently succeeded only in the analysis of the first-NN shells in the Pt $L_{\mathrm{III}}$-edge EXAFS and the first- to third-NN shells in the I $K$-edge EXAFS, all of which show intense EXAFS oscillations up to sufficiently high $k$ regions.

The filtered $k^2\chi(k)$ for the first- to third-NN shells in the I $K$-edge EXAFS of $K_2PtI_6$ are shown in Fig. 3. One can find the amplitude reduction at higher temperatures, which originates from the enhancement of $C_2$. The phase delay is also found especially for the second-NN shell [Fig. 3(b)], which is associated with $C_3$. In the analysis of the second- and third-NN shells of the I $K$-edge EXAFS, we also assumed

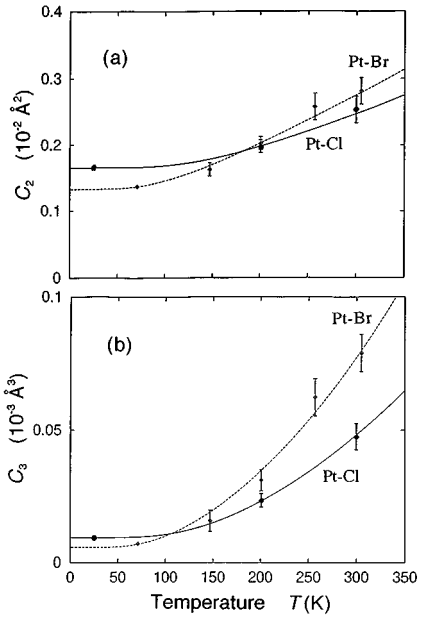


FIG. 4. Temperature dependence of (a) $C_2$ and (b) $C_3$ for the first-NN Pt-Cl shell of $PtCl_6^{2-}$ (solid circles for experimental data and solid line for calculated data) and for the first-NN Pt-Br shell of $PtBr_6^{2-}$ (open circles and dashed line). For the experimentally obtained $C_2$ and $C_3$, the calculated values at the lowest temperatures (25 K for $PtCl_6^{2-}$ and 71 K for $PtBr_6^{2-}$) are added.

the single-shell contributions. For the I-I′ pair, we have neglected multiple-scattering contributions such as a triangular I-Pt-I′-I path ($\angle$IPtI′$=90°$), as mentioned above. For the third-NN I-Pt-I′-Pt-I shell, all the paths except the $\angle$IPtI′$=180°$ cases have been neglected. Since these three collinear components (single-, double-, and triple-scattering I-Pt-I′ paths) show exactly the same cumulants,[8] we can perform the single-shell analysis similarly to the first-NN analysis. $C_2$ and $C_3$ of the first-NN Pt-$X$ shells in $PtCl_6^{2-}$ and $PtBr_6^{2-}$ are plotted in Fig. 4 and the results of the first- to third-NN shells of $PtI_6^{2-}$ are depicted in Fig. 5, where the calculated values discussed below are also given. In Figs. 4 and 5, the calculated $C_2$ and $C_3$ values at the lowest temperature were added to the experimentally obtained $\Delta C_2$ and $\Delta C_3$ to yield the absolute values at higher temperatures. The temperature dependence of $\Delta R$ is so small as the error bar, and is omitted because of less reliability for quantitative discussion of the interatomic potential.

### C. Force constants

The analysis of $C_2$ can be performed with the harmonic approximation. For $PtCl_6^{2-}$ and $PtBr_6^{2-}$, $K$, $F$, and $H$ have been given by the vibrational data and we can straightforwardly evaluate $C_2$ for the first-NN Pt-Cl or Pt-Br shell. As shown in Fig. 4(a), the experimental data given by EXAFS agrees quite well with the expected values, indicating that $C_2$ is correctly provided with the harmonic interatomic potential determined by the vibrational data. For $Pt_6^{2-}$, because of lack of a Raman spectrum we have only two IR frequencies, implying one more experimental datum required. Here we have employed $C_2$ for the first-NN I-Pt shell, which is dependent on $K$ and $F$. These three experimental data lead to

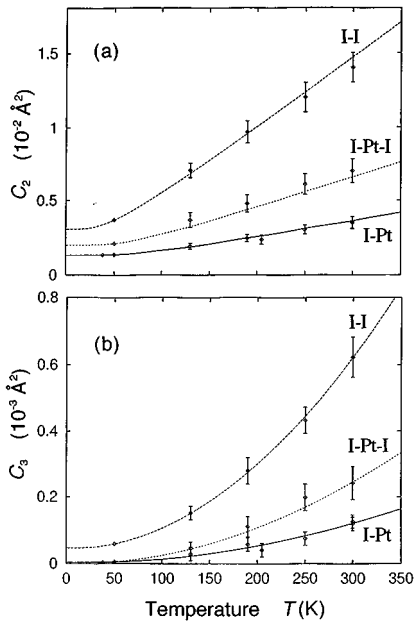


FIG. 5. Temperature dependence of $C_2$ and $C_3$ for the first-NN I-Pt (solid line), the second-NN I-I (long-dashed), and the third-NN I-Pt-I (short-dashed) shells. Data points with error bars correspond to the experimental data given by the Pt $L_{\mathrm{III}}$- and I $K$-edge EXAFS analyses. For the experimentally obtained $C_2$ and $C_3$, the calculated values at the lowest temperatures (38 K for Pt $L_{\mathrm{III}}$ and 50 K for I $K$) are added in order to compare the calculated lines.

the harmonic force constants, as given in Table II. In the case of I $K$-edge EXAFS, we can also discuss $C_2$ of the second- and third-NN shells. For the second-NN I-I shells, Fig. 5(a) shows excellent agreement between the experimental and calculated values, while the calculation for the third-NN I-Pt-I shell is found to underestimate $C_2$ slightly. Although this might be within the error bars, the slight deviation would arise from somewhat poor approximation of the **GF** matrix in Eq. (1), in which several kinds of cross terms are described using only one parameter $F$.

In order to discuss the contribution of the bending motion to $C_2$ of the second-NN I-I shell, let us neglect the bending force constant $H$ in the calculation. $C_2$ at 300 K is thus estimated to be $1.69\times10^{-2}$ Å$^2$, which is by 15% larger than the value of $1.47\times10^{-2}$ Å$^2$, obtained by the appropriate analysis including $H$. $C_2$ of the first-NN shell also changes by 2% due to the coupling of the $F_{1u}$ stretching and bending modes, while $C_2$ of the third-NN shell does not vary at all. These results imply that the contribution of the bending mode plays a minor role even for the second-NN I-I shell where the bending mode directly affects.

For the determination of the anharmonic potential parameters, let us first neglect the cross terms concerning $F_3$. From the first-NN Pt-$X$ shells, one can determine $K_3$ in the absence of $F_3$ because the bending anharmonicity $H_3$ does not affect the first-NN shell. The obtained values are tabulated in Table II. Although in the cases of $PtCl_6^{2-}$ and $PtBr_6^{2-}$ one cannot include $F_3$ because of a lack of the other NN information, the analysis of $PtI_6^{2-}$ can be performed using $C_3$ of the third-NN I-Pt-I shell. It might be quite important to take $F_3$ into account since in the analysis of the vibrational data the harmonic force constant $F$ plays an essentially important role. Actually in the absence of the $F$ contribution the $C_3$ values of the first-NN I-Pt and the third-NN I-Pt-I shells are not consistent with each other; $C_3$ of the third-NN shell was found to be by as much as ~40% underestimated assuming $F_3=0$. In order to obtain $F_3$, we should give some assumption of $F_3$, which has basically four different types in the octahedral system. Here we have tried two possibilities; first all $F_3$ values are assumed to be the same, and second $F_{3,lmn}$ $(l\neq m\neq n)$ is neglected and the other $F_3$ values are assumed to be the same. These two assumptions do not exhibit noticeable difference in the bending contribution discussed below and we will thus hereafter mention the results only in the case that all the $F_3$ values are equal to each other. On that condition, as given in Table II, one can consequently estimate $K_3=2.5(3)$ (mdyn/Å$^2$) and $F_3=1.1(2)$ (mdyn/Å$^2$) from $C_3$ of the first- and third-NN shells of $PtI_6^{2-}$. Since the resultant $K_3$ value was slightly modified comparing to $K_3=2.2$ (mdyn/Å.$^2$) obtained in the analysis of the first-NN shell assuming $F_3=0$, these previous values should be regarded as effective ones. Figure 5 shows also the $C_3$ curves of the first- and third-NN shells calculated including $F_3$.

With the assumption of $K_3$and $F_3$ obtained above, $H_3$ is immediately calculated from $C_3$ of the second-NN I-I shell as 0.021(2) (mdyn/Å$^2$). As mentioned above, the second-NN I-I shell contains information on $K_3$, $F_3$, and $H_3$. When we neglect $H_3$ and take only $K_3$ and $F_3$ into account for the second-NN I-I shell, the $C_3$ value at 300 K is estimated to be $0.454\times10^{-3}$ Å$^2$, which is by 19% smaller than the appropriate value of $0.562\times10^{-2}$ Å$^2$. Note that $C_3$ of the first- and third-NN shells are not at all dependent on $H_3$. The present results imply that the anharmonicity of the I-I shell originates mainly from the stretching mode (~81%) and partly from the bending vibration, this being a similar conclusion to the $C_2$ case (~85%).

TABLE II. Second- and third-order force constants of $PtCl_6^{2-}$, $PtBr_6^{2-}$, and $PtI_6^{2-}$. The second-order constants $K$, $F$, and $H$ (mdyn/Å units) were determined by the vibrational spectra. For $PtI_6^{2-}$, since the Raman data are not available, we used the IR frequencies and the EXAFS results of $\Delta C_2$ for the first-NN Pt-I shell to determine the constants. The third-order constants $K_3$,$F_3$, and $H_3$ (mdyn/Å$^2$ units) were given by the present EXAFS analysis. For the determination of $K_3$ of $PtCl_6^{2-}$ and $PtBr_6^{2-}$, $F_3=0$ was assumed, while for $PtI_6^{2-}$ both results are given.

| | Harmonic | | | Anharmonic | | |
|---|---|---|---|---|---|---|
| Sample | $K$ | $F$ | $H$ | $K_3$ | $F_3$ | $H_3$ |
| $PtCl_6^{2-}$ | 1.829 | 0.148 | 0.0938 | 3.4(7) | (0.0)[a] | |
| $PtBr_6^{2-}$ | 1.485 | 0.138 | 0.0291 | 3.7(4) | (0.0)[a] | |
| $PtI_6^{2-}$ | 1.00 | 0.20 | 0.019 | 2.2(3) | (0.0)[a] | |
| | 1.00 | 0.20 | 0.019 | 2.5(3) | 1.1(2) | 0.021(2) |

[a] $F_3$ is neglected.

## V. CONCLUSIONS

We have derived the formulas to give cumulants determined by EXAFS, assuming the third-order anharmonic potential with a general form. Although we have investigated

the octahedral system here, these formulas can basically be applied to any molecular structure. In the $PtX_6^{2-}$ system studied, $C_2$ agrees with the values expected from the vibrational data not only for the first-NN shells but for the second- and third-NN coordinations. The third-order Pt-$X$ stretching force constants $K_3$ have successfully been determined from $C_3$ of the first-NN Pt-$X$ shells, if we neglect the cross terms concerning $F_3$. From the I $K$-edge EXAFS analysis of $PtI_6^{2-}$, we have also obtained information on the anharmonicity of the second- and third-NN shells. $C_3$ of the third-NN I-PT-I shell indicated that the force constant $F_3$ should be included, consequently leading to the $K_3$ and $F_3$ values. The resultant $K_3$ value is slightly modified. For the second-NN I-I shell in $PtI_6^{2-}$, we have discussed the contribution of the bending modes and found that for both $C_2$ and $C_3$, the bending vibrations concerning $H$ and $H_3$ play minor roles and the stretching modes are more important.

## ACKNOWLEDGMENTS

The present authors gratefully acknowledge K. Kobayashi, H. Hamamatsu, S. Takenaka, and O. Endo for their help during the EXAFS measurements. We are also grateful to the Photon Factory staffs, Professor M. Nomura and Dr. N. Usami, who are in charge of Beamlines 7C and 10B. This work was carried out under the approval of Photon Factory Program Advisory Committee (PF-PAC No. 94G226).

[1] See, for instance, *X-Ray Absorption: Principles, Applications, Techniques of EXAFS, SEXAFS and XANES*, edited by D. C. Koningsberger and R. Prins (Wiley, New York, 1988).

[2] G. Bunker, Nucl. Instrum. Methods **207**, 437 (1983).

[3] See, for instance, T. Yokoyama, T. Satsukawa, and T. Ohta, Jpn. J. Appl. Phys. **28**, 1905 (1989); T. Yokoyama and T. Ohta, *ibid.* **29**, 2052 (1990); L. Tröger, T. Yokoyama, D. Arvanitis, T. Lederer, M. Tischer, and K. Baberschke, Phys. Rev. B **49**, 888 (1994).

[4] T. Yokoyama, H. Hamamatsu, Y. Kitajima, Y. Takata, S. Yagi, and T. Ohta, Surf. Sci. **313**, 197 (1994); T. Lederer, D. Arvanitis, M. Tischer, G. Comelli, L. Tröger, and K. Baberschke, Phys. Rev. B **48**, 11 277 (1993).

[5] H. Rabus, Ph.D. thesis, Freie Universität Berlin, 1991.

[6] A. I. Frenkel and J. J. Rehr, Phys. Rev. B **48**, 585 (1993).

[7] T. Fujikawa and T. Miyanaga, J. Phys. Soc. Jpn. **62**, 4108 (1993); T. Miyanaga and T. Fujikawa, **63**, 1036 (1994).

[8] T. Yokoyama, K. Kobayashi, T. Ohta, and A. Ugawa, Phys. Rev. B **53**, 6111 (1996).

[9] H. Oyanagi, T. Matsushita, M. Ito, and H. Kuroda (unpublished); M. Nomura (unpublished).

[10] M. Nomura and A. Koyama (unpublished).

[11] H. C. Urey and C. A. Bradley, Phys. Rev. **38**, 1969 (1931).

[12] K. Nakamoto, *Infrared Spectra of Inorganic and Coordination Compounds*, 4th ed. (Wiley, New York, 1986); C. W. F. Pistorius, J. Chem. Phys. **29**, 1328 (1958).

[13] J. Hiraishi and T. Shimanouchi, Spectrochim. Acta **22**, 1483 (1966); D. M. Adams and D. M. Morris, J. Chem. Soc. A **1967**, 1666 (1967); J. Hiraishi, I. Nakagawa, and T. Shimanouchi, Spectrochim. Acta **20**, 819 (1964).

[14] T. Yokoyama, H. Hamamatsu, and T. Ohta, EXAFS Analysis Program EXAFSH Ver. 2.1, The University of Tokyo, 1993.

[15] J. J. Rehr, J. Mustre de Leon, S. I. Zabinsky, and R. C. Albers, J. Am. Chem. Soc. **113**, 5135 (1991); S. I. Zabinsky, J. J. Rehr, A. Ankdinov, R. C. Albers, and M. J. Eller, Phys. Rev. B **52**, 2995 (1995).

[16] H. Takazawa, S. Ohba, and Y. Saito, Acta Crystallogr. Sect. B **46**, 166 (1990).

[17] G. Thiele, C. Mrozek, D. Kamerer, and K. Wittmann, Z. Naturforsch Teil B **38**, 905 (1983).